Fibrillation of Carrier Protein Albebetin and Its Biologically Active Constructs. Multiple Oligomeric Intermediates and Pathways†

Ludmilla A. Morozova-Roche,*,‡,§ Vladimir Zamotin,‡,§ Mantas Malisauskas,‡ Anders Öhman,|| Rita Chertkova,⊥ Marika A. Lavrikova,⊥ Irina A. Kostanyan,⊥ Dmiltry A. Dolgikh,⊥ and Michail P. Kirpichnikov⊥

Department of Medical Biochemistry and Biophysics, Umeå University, Umeå, SE-90187 Sweden, Department of Biochemistry, Umeå University, Umeå, SE-90187 Sweden, and Shemyakin and Ovchinnikov Institute of Bioorganic Chemistry, Russian Academy of Sciences, Moscow, Russia

Received March 26, 2004; Revised Manuscript Received May 30, 2004

ABSTRACT: We showed that the genetically engineered carrier-protein albebetin and its biologically active constructs with interferon-α_2 octapeptide LKEKKYSP or differentiation factor hexapeptide TGENHR are inherently highly amyloidogenic at physiological pH. The kinetics of fibrillation were monitored by thioflavine-T (ThT) binding and the morphological changes by atomic force microscopy. Fibrillation proceeds via multiple pathways and includes a hierarchy of amyloid structures ranging from oligomers to protofilaments and fibrils. Comparative height and volume microscopic measurements allowed us to identify two distinct types of oligomeric intermediates: pivotal oligomers ca. 1.2 nm in height comprised of 10−12 monomers and on-pathway amyloid-competent oligomers ca. 2 nm in height constituted of 26−30 molecules. The former assemble into chains and rings with "bead-on-string morphology", in which a "bead" corresponds to an individual oligomer. Once formed, the rings and chains remain in solution simultaneously with fibrils. The latter give rise to protofilaments and fibrils, and their formation is concomitant with an increasing level of ThT binding. The amyloid nature of filamentous structures was confirmed by a pronounced ThT and Congo red binding and β-sheet-rich far-UV circular dichroism. We suggest that transformation of the pivotal oligomers into the amyloid-prone ones is a limiting stage in amyloid assembly. Peptides, either fused to albebetin or added into solution, and an increased ionic strength promote fibrillation of albebetin (net charge of −12) by counterbalancing critical electrostatic repulsions. This finding demonstrates that the fibrillation of newly designed polypeptide-based products can produce multimeric amyloid species with a potentially "new" functionality, raising questions about their safety.

Over the past decade, unprecedented progress achieved in biomolecular engineering has led to the discovery and rational design of polypeptide-based materials in diverse areas of pharmaceutical, biomedical, agricultural, and environmental applications. The frequency of therapeutic interventions with high-value *de novo* molecules, including drug delivery of biologically active peptides, enzymes, and vaccines, will continue to increase (*1*, *2*). In the past several years, a large body of evidence has also accumulated suggesting that the assembly of soluble proteins and peptides into ordered amyloid structures is not limited to the pathology of human diseases such as Alzheimer's and Parkinson's diseases or systemic amyloidoses but is a generic property of the polypeptide backbone (*3*). Indeed, numerous proteins, including such well-known ones as lysozymes, α-lactalbumin, myoglobin (*4*−*7*), and others, can be prompted to adopt amyloid-type architecture with a characteristic cross-β-sheet core under destabilizing conditions either *in vivo* or *in vitro*. Given the universal character of amyloid conformation and the variety of conditions existing in the body, the questions arise whether such species can be evoked in *de novo*-designed protein-based therapeutics and which properties of the precursor states can promote such a conversion.

To address this problem, we studied the amyloidogenicity of carrier-protein ABB[1] and its genetically engineered constructs ABBI and ABB-DF. ABB is characterized by a double repeat of the $\alpha\beta\beta$ motif (*8*, *9*) arranged in such a way that four β-strands form an antiparallel β-sheet covered by α-helices (Figures 1 and 2). The compactness of ABB was optimized by the short loops connecting the elements

† The financial support provided by grants from the Swedish Medical Research Council, the Kempe Foundation to purchase atomic force microscope, and the RAS program on physicochemical biology is gratefully acknowledged. L.A.M.-R. is supported by the Swedish Medical Research Council and M.M. by the Sven and Lilly Lawskis Foundation. M.A.L. acknowledges the contribution from the Visby Programme of the Swedish Institute.

* To whom correspondence should be addressed: Department of Medical Biochemistry and Biophysics, Umeå University, Umeå, SE-90187 Sweden. Phone: +46 90 786 52 83. Fax: +46 90 786 97 95. E-mail: Ludmilla.Morozova-Roche@chem.umu.se.

‡ Department of Medical Biochemistry and Biophysics, Umeå University.

§ These authors contributed equally to this work.

|| Department of Biochemistry, Umeå University.

⊥ Russian Academy of Sciences.

[1] Abbreviations: ABB, albebetin; ABBI, albebetin with the grafted LKEKKYSP (131−138) octapeptide from interferon-α_2; ABB-DF, albebetin with the grafted TGENHR (41−46) hexapeptide from the differentiation factor for the HL-60 cell line of human promyelocyte leukemia; AFM, atomic force microscopy; ANS, 1-anilinonaphthalene-8-sulfonate; CD, circular dichroism; HLDF-6, TGENHR (41−46) hexapeptide from the human leukemia differentiation factor; ThT, thioflavine-T; UV, ultraviolet.

10.1021/bi0494121 CCC: $27.50 © 2004 American Chemical Society
Published on Web 07/08/2004

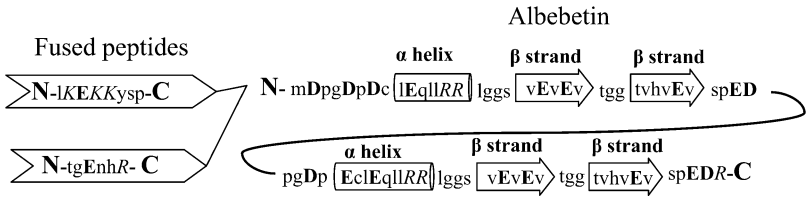

FIGURE 1: Primary structure of ABB. Peptides of interferon-α_2 or HLDF-6 fused to ABB are shown as arrows. Amino acid residues with positively charged side chains at pH 7.3 are denoted with italic capital letters, and those with negatively charged groups are denoted with bold capital letters.

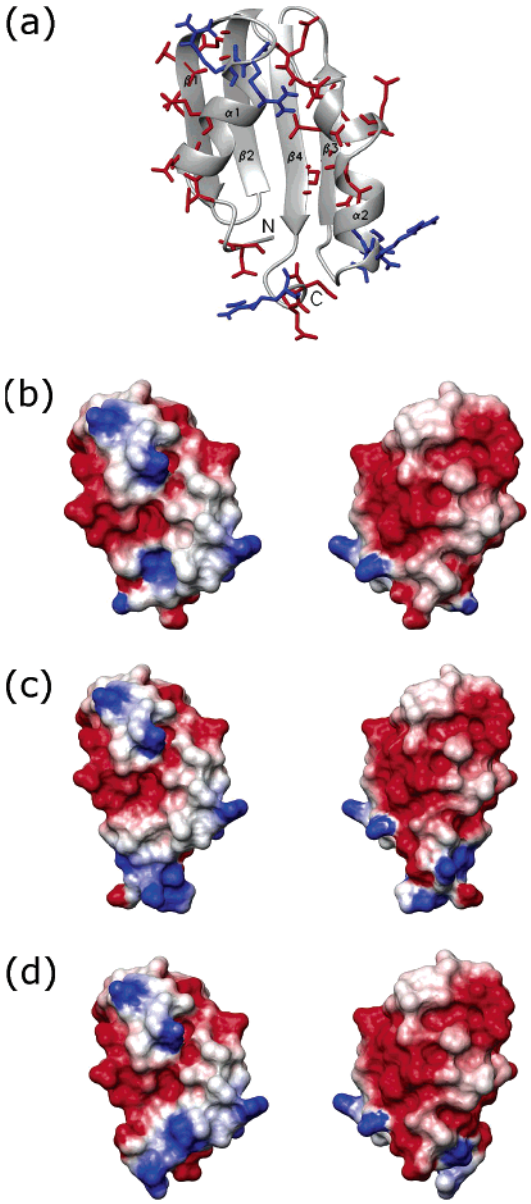

FIGURE 2: Structural modeling of ABB proteins. (a) Ribbon representation of the ABB molecule, where positively and negatively charged side chains are shown in blue and red, respectively. The same color coding is used for the calculated electrostatic surface potentials of ABB (b), ABBI (c), and ABB-DF (d). The molecules on the left-hand side of panels b−d are oriented in a manner identical to that of panel a, while the molecules on the right-hand side have been rotated 180° around a vertical axis. Figures were prepared by using MOLMOL (*42*).

of the secondary structure and limiting the number of conformations which can be adopted. While ABB possesses a well-defined secondary structure, it is characterized by a labile tertiary structure, which correlates with its low immunogenicity (*10*). To prevent ABB from aggregating, the charged residues were introduced into all elements of its secondary structure, creating a net charge of −12 (Figure 2).

In controlled drug delivery, a variety of therapeutic agents such as small molecules, peptides, proteins, and oligonucleotides are conjugated to carrier-proteins, which are able to protect the labile compounds from degradation and also to reduce their immunogenicity (*2*, *11*, *12*). For this purpose, the LKEKKYSP octapeptide of human interferon-α_2 or the TGENHR hexapeptide of the human leukemia differentiation factor were fused to the N-terminus of ABB (*10*, *13*, *14*), which resulted in two biologically active constructs possessing the functionality of the fused peptides. The first construct, ABBI, activates the thymocyte blast transformation in a manner similar to that of interferon-α_2 (*15*), while the second, ABB-DF, induces the differentiation and inhibits proliferation of human leukemia cells in a manner similar to that of molecules of the differentiation factor (*14*, *16*). The inserted sequences also produced a very pronounced effect on the amyloidogenic properties of ABB, providing insight into the molecular forces driving amyloid formation.

EXPERIMENTAL PROCEDURES

Protein Samples. The designed proteins ABB, ABBI, and ABB-DF were expressed in *Escherichia coli* as described previously (*9*, *13*, *14*). The protein concentration was determined by the absorbance measurement at 280 nm using an extinction coefficient $E_{1\%}$ of 3 for both ABB and ABB-DF and an $E_{1\%}$ of 17 for ABBI, calculated using the amino acid composition of the proteins. To initiate fibrillation, the solutions of proteins and HLDF-6 peptide were prepared at a concentration of 20 mg/mL in 20 mM bis-Tris buffer and 0.2% sodium azide (pH 7.3).

Structure Modeling. Structural models of the *de novo*-designed proteins were constructed using the Swiss-Pdb-Viewer program for alignment (version 3.7; www.expasy.ch/spdbv/) (*17*) and the optimise mode of the SWISS-MODEL program server for automatic model building (version 3.5; www.expasy.ch/swissmod/SWISS-MODEL.html). They were based on the obtained sequence alignments and recognized folds found by the 3D-Jury method (*18*) at the MetaServer (www.bioinfo.pl). The fold of ABB was modeled in comparison with those of three RNA-binding proteins (PDB entries 1B7F, 1D8Z, and 1QMH), while the modeling ABBI and ABB-DF structures included the coordinates of two additional RNA-binding proteins (PDB entries 1CVJ and 1JMT). The evaluation of the quality of the models as well as their visualization was carried out as previously described (*19*).

Amyloid Assays. The ThT binding assay was performed using a modification of the method of Levine (*20*, *21*). Fluorescence measurements were carried out on a Fluoro-

Max-2 spectrofluorometer (JOBIN YVON/SPEX Instruments SA). The fluorescence of ThT was excited at 440 nm, and the emission spectrum was recorded between 450 and 550 nm, setting the excitation and emission slits at 5 nm.

The Congo red binding assay was performed according to the procedure described in refs *22* and *23*. Optical spectra were recorded on a Beckman UV spectrophotometer; the spectra of the reaction solution were collected together with negative controls containing dye and protein separately, subtracting from the former the signals associated with the absorption of the dye and the scattering contribution from the fibrils.

Spectroscopic Methods. CD spectra were collected on a Jasco J720 CD UV spectrometer equipped with a water bath temperature controller using a 1 mm light path quartz cell.

The fluorescence of ANS was measured on a FluoroMax-2 spectrofluorometer with excitation at 365 nm and emission at 470 nm and setting 10 nm spectroscopic slits for both excitation and emission.

AFM. AFM measurements were performed on PICO SPM (Molecular Imaging) and Nanoscope IIIa Multi-Mode microscopes (Digital Instruments) in a tapping mode using acoustically driven cantilevers. The radius of curvature of the AFM tips was less than 10 nm (Atomic Force). Scanners with a 100 μm scan size were used in both instruments. Before images were recorded, the scanner was calibrated by using a standard 1 μm calibration grid (Molecular Imaging) in the $x-y$ plane and measuring atomic steps on a highly oriented pyrolytic graphite surface in the z axis.

Etched silicon probes attached to triangular cantilevers 100−200 μm in length (NanoDevices, Metrology Probes Inc.) with a nominal spring constant of 35 N/m were operated at resonance frequencies of 100−200 kHz. The scan rate was in the range of 1−3 Hz depending on the scan size with a resolution of 256 and 512 pixels. Height, amplitude, and phase data were collected simultaneously. The scanning of samples was performed in trace and retrace to avoid the scan artifacts. The cross-section analysis in the height images was carried out to determine the dimensions of amyloid structures.

For ambient imaging of amyloid samples, we followed the preparation procedure described previously (*5*). The incubation samples were diluted up to 1000 times to the final concentration of 20−100 μg/mL, placed on the surface of freshly cleaved mica (GoodFellow), left for 3 min, rinsed three times with MilliQ water, and dried by evaporation in air at room temperature overnight. Thus, the time exposure of the original sample to the mica substrate (3 min) was significantly shorter than the amyloid incubation time (hours and days). Taken together with the strong dilution of the incubation samples, these ensured that aggregation or fibril formation was not triggered or affected by the mica surface. To evaluate the effect of imaging environment and the substrate surface on amyloid structures, the control measurements were performed under ambient and liquid conditions using both mica and graphite as substrates. Previous investigations suggested that behavior of adsorbed protein structures is not a general phenomenon and each protein−surface combination must be examined individually (*24*, *25*). Topographical images of amyloid oligomers and fibrils were essentially the same under all conditions. However, due to electrostatic repulsion between the mica surface and highly negatively charged ABB structures, we have increased adsorption time to 30−40 min prior to recording images in MilliQ water to produce the same population density of amyloid structures as under ambient conditions. Alternatively, we have achieved a similar effect by adding 100 mM NaCl to the imaging solution with preformed amyloid species but keeping the adsorption time to 3 min. The adsorption of ABB structures to graphite in water was also rather poor, resulting in a low population density of oligomers and fibrils on the substrate even after adsorption for 40 min. To reduce adsorption time and avoid artifacts induced by salt during scanning, we have selected ambient conditions and a mica substrate for further measurements.

Molecular Volume Calculation. The volume of protein species was derived from AFM images as described in ref *26*. Because of adhesion forces, all multimeric complexes were spread on the mica substrate, giving larger lateral dimensions than vertical measurements. Generally, AFM also overestimates the lateral dimensions of biological samples due to the geometry of the tip, which induces a broadening effect in the image. To determine the actual tip geometry and the accuracy of our measurements, we used the tip deconvolution module of the Scanning Probe Image Processor (SPIP) (Image Metrology) and performed measurements on the reference samples such as carbon nanotubes ca. 1 nm in diameter, spherical latex particles ca. 1.5 nm in diameter, and individual molecules of equine lysozyme (*5*). Processing images with the SPIP tip deconvolution module indicated that there were no topological artifacts due to the shape of the tip. Measurements of the reference samples confirmed the suggestion made in refs *26* and *27* that the diameter at half-maximal height of individual particles sufficiently compensates for the AFM-induced overestimation of lateral dimensions of protein structures.

The height and half-height diameters of the amyloid oligomers were measured from multiple cross sections of the same particle, which was treated as a spherical cap. The volume of each particle was calculated using the following equation (*26*, *27*):

$$V_{AFM} = (\pi h/6)(3r^2 + h^2) \quad (1)$$

where h is the particle height and r is the radius at half-height.

The molecular volume of monomeric proteins was calculated using the equation (*26*, *27*)

$$V_m = (M_o/N_o)(V_1 + dV_2) \quad (2)$$

where M_o is the protein molecular weight, N_o is Avogadro's number, d is the extent of protein hydration (0.4 mol of H_2O/mol of protein), and V_1 and V_2 are the partial specific volumes of the individual protein (0.74 cm^3 g^{-1}) and water (1 cm^3 g^{-1}) molecules, respectively. The molecular volumes of equine lysozyme estimated from AFM measurements by using eq 1 and calculated by using eq 2 gave a good agreement. The calculated molecular volumes of ABB, ABBI, and ABB-DF are 14.8, 16.7, and 16.1 nm^3, respectively.

The number of monomers in oligomeric species was determined by the equation

$$n = V_{AFM}/V_m \quad (3)$$

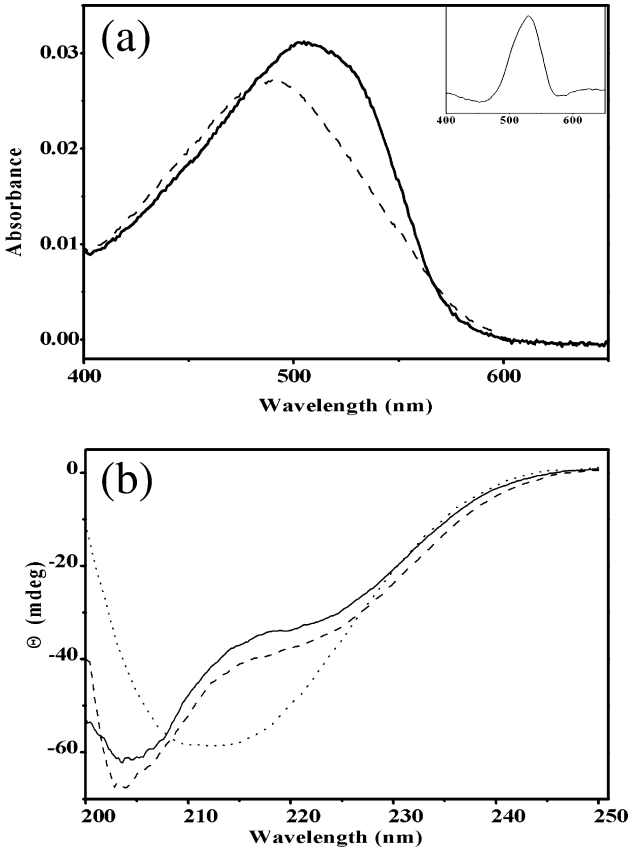

FIGURE 3: Spectroscopic assays of fibril formation of ABB-based proteins. (a) The absorption spectra of the Congo red dye bound to ABB protofilaments (—) and in the absence of ABB (- - -). The shift of the absorption spectrum is more clearly presented (inset) by subtracting the latter and the scattering light caused by protofilaments alone from the former. (b) The far-UV CD spectra of the freshly prepared ABB-DF at 20 (—) and 57 °C (- - -), at a protein concentration of 0.2 mg/mL, with 20 mM bis-Tris buffer (pH 7.3) and 0.2% sodium azide. The spectrum of ABB-DF amyloid fibrils (···) recorded after incubation for 4 days at 57 °C.

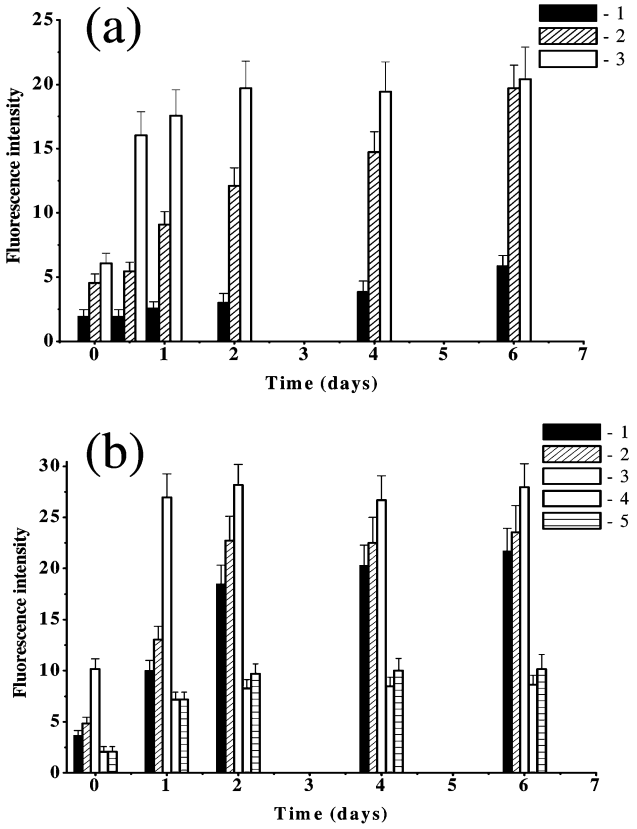

FIGURE 4: Kinetic of amyloid formation of ABB-based proteins monitored by ThT fluorescence. (a) Time dependence of amyloid formation of ABB (1), ABBI (2), and ABB-DF (3). (b) Time dependence of amyloid formation of ABB (1), ABBI (2), and ABB-DF (3) in the presence of an equimolar concentration of HLDF-6 and of ABB in the presence of 100 (4) and 200 mM NaCl (5). Each data set represents a mean value of four measurements.

RESULTS

Spectroscopic Assays for Amyloid Formation. The formation of fibrils during incubation of ABB, ABBI, and ABB-DF at pH 7.3 and 57 and 23 °C (room temperature) was detected by ThT and Congo red dye binding assays, used as classic markers of amyloid (*20*−*23*). The 10 μM aliquots of all proteins were added to the solution containing ThT, and subsequently, we measured a 1 order of magnitude enhancement of the fluorescence signal compared to the fluorescence of the free dye after incubation for a few days at 57 °C. A similar effect was observed after incubation of ABBI and ABB-DF for 4 days at 23 °C. ThT fluorescence was not changed even after incubation of ABB for 24 days at 23 °C. The interaction of the amyloid fibrils of ABB and ABB-based constructs with the dye Congo red produced a significant red shift of the light absorbance spectrum of Congo red. The representative spectrum of Congo red in the presence of ABBI demonstrating the shift from 495 to 505 nm is shown in Figure 3a.

Both ABB and ABB-based constructs were characterized by very similar far-UV CD spectra, and the representative spectrum of ABB-DF is shown in Figure 3b. This indicated that fusing the peptides to the N-terminus of ABB did not affect its secondary structure. Heating the sample of ABB-DF to 57 °C did not perturb the far-UV CD spectrum as shown in Figure 3b; the secondary structure of ABB and ABBI were also unchanged at the higher temperature. The high degree of conformational flexibility of ABB and its constructs was consistent with a pronounced random-coil CD signal at 200−210 nm. The formation of fibrils, by contrast, was manifested in significant changes in the far-UV CD spectra of individual proteins, revealing a substantial increase in β-sheet content (Figure 3b).

The interaction of ABB and the constructs with the hydrophobic dye ANS was probed by measuring ANS fluorescence at both 23 and 57 °C. The fluorescence did not change under either condition compared to the dye free in solution, indicating the absence of extended hydrophobic patches (*28*) on the protein molecules that are able to bind ANS, and heating did not increase the level of exposure of such hydrophobic surfaces. However, heating increases the conformational mobility of the protein structure which can prompt protein to enter an alternative pathway and facilitate assembly into amyloid fibrils. A further increase in temperature would lead to unfolding of the secondary structure and subsequently nonstructured aggregation. This is why we selected 57 °C as a second condition for amyloid formation.

Kinetics of Amyloid Formation. The time dependence of fibril formation was monitored by measuring an enhancement of ThT fluorescence bound to the aliquots of protein samples collected at differing time intervals (Figure 4). The intensity of ThT fluorescence remained at the same level when ABB was incubated for up to 12 h, indicating a distinct lag phase.

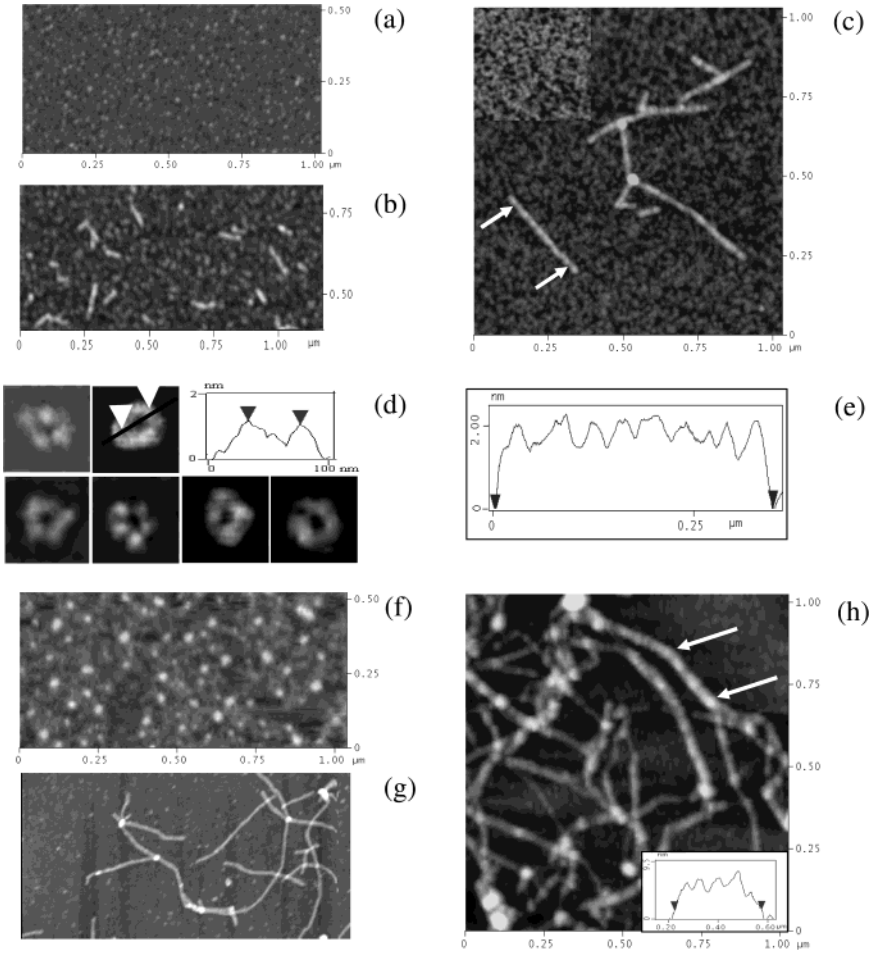

FIGURE 5: Amyloid assemblies of ABB observed by AFM. (a) Height image of pivotal oligomers ca. 1.2 nm in height, during day 1 of incubation, at pH 7.3 and 57 °C. The *z* scale is 5 nm. (b) Chain and ring oligomeric assemblies of amyloid-prone oligomers ca. 2 nm in height and protofibrils, on day 2, with a *z* scale of 5 nm. (c) Height image of protofilaments recorded on day 7, with a *z* scale of 5 nm. Insertion in the left corner shows the rings and the chains at a *z* scale of 3 nm. (d) Panel of 100 nm × 100 nm images of individual rings illustrating that they are composed of four or five oligomers. The cross-sectional analysis of an individual ring (top right panel). Cursors indicate the highest points on the ring wall. (e) Cross section of the ABB protofilament made along its axis (panel c) and marked by cursors. It demonstrates that the *z* height is ca. 2 nm and the period of twist is ca. 40 nm. (f) Granules of ABB formed at 23 °C on day 24, with a *z* scale of 10 nm. (g) Amyloid fibrils formed at 57 °C in the presence of 200 mM NaCl, with a *z* scale of 10 nm. (h) Network of ABB fibrils formed in the presence of HLDF-6, with a *z* scale of 15 nm. The inset shows the cross section of an individual fibril along its axis relative to the mica substrate; the maxima and minima are 8.0 ± 0.5 and 6 ± 0.5 nm, respectively. The distance between the maximum heights is 60 ± 5 nm.

During this stage, only round oligomers were detected in the sample by AFM. Subsequently, a gradual increase in the level of ThT binding was observed in the course of 1 week (Figure 4a), indicating an appearance and accumulation of amyloid structures confirmed by AFM analysis. Fibrillation of the ABB constructs proceeded more rapidly, resulting in a pronounced increase in ThT fluorescence within hours of incubation for 12 h (Figure 4a). The plateau level of ThT fluorescence was significantly (5-fold) higher in the latter than in the sample containing the ABB fibrils. In the case of ABB-DF, the plateau level of ThT fluorescence was reached after incubation for 2 days in contrast to the period of 6 days required for ABBI.

An equimolar addition of the HLDF-6 peptide to the solutions with the monomeric ABB-DF did not change the kinetics of amyloid formation, but the level of ThT fluorescence at the stationary phase increased compared to that of ABB-DF incubated in the absence of the peptide (Figure 4b). The fibrillation of ABB and ABBI proceeded significantly faster in the presence of HLDF-6, reaching the level of plateau in 2 days (Figure 4b), and the magnitude of fluorescence intensity at the plateau was the same as for ABB-DF (Figure 4a).

All three proteins were also incubated in the presence of 100 and 200 mM NaCl. An increased ionic strength did not affect the kinetics of ABBI and ABB-DF amyloid formation. By contrast, in the presence of salt in the sample with the ABB protein, the plateau level of ThT was reached in 2 days and was 2 times higher than in the absence of salt, but remained 2−2.5-fold lower than that for ABB constructs (Figure 4a,b).

AFM Imaging of Amyloid Structures. AFM is a powerful tool for monitoring the process of amyloid formation (Figures 5 and 6). Within hours of dissolving, all three ABB proteins formed round oligomers presented in the AFM images as round specks (Figures 5a and 6a). The population density, i.e., more oligomers on the mica surface, increased progressively during incubation as shown for ABB for a period of 1 week (Figure 5a−c). Their *z* height measured in a cross section was 1.2 ± 0.3 nm, and the *x*−*y* dimension measured at a half-height was 18 ± 3 nm. These oligomers were composed of 8−10 protein molecules calculated by using

eqs 1−3 and were defined as pivotal ones. They assembled subsequently into the linear chains comprised of two to six round units or into rings (locked chains) (Figure 5b−d). The rings were characterized by a diameter of 45 ± 10 nm measured between the maximal heights of their walls and by an oscillating height along the circumference with the maximal values of ca. 1.2 nm (Figure 5d). They were apparently made up of four or five pivotal oligomers. Individual amyloid rings were observed under ambient conditions on both the mica and graphite substrates by using a 10 000 times higher dilution of the initial incubation sample, confirming that they were sampled from solution but not assembled during exposure to the surface. The proportion of the rings versus the chains increased in the samples of all three proteins during the course of incubation (Figure 5b,c), though both of them remained in large quantities at the later stages of incubation when mature fibrils had accumulated.

Larger round oligomers with a *z* height of 2.0 ± 0.3 nm and an *x*−*y* dimension at half-height of 25 ± 5 nm emerged in the sample of ABB after 1 day (Figure 5b) and in the ABBI and ABB-DF solutions within hours of incubation (Figure 6a). They consisted of 26−30 monomeric proteins as estimated by using eqs 1−3. In the sample of ABB, well-segmented protofibrils were formed on day 2 of incubation (Figure 5b). They consisted of a few repetitive (a minimal number of 2) units ca. 2 nm in height. Filamentous structures of ABB with a length distribution between 100 and 500 nm and a *z* height of ca. 2 nm were monitored after incubation for 3 days and more (Figure 5c). Such a *z* dimension corresponds to a minimal cross-sectional parameter of single-stranded fibrils categorized as protofilaments (*29*). A periodic repeat of 20−40 nm was measured along the main axis of the protofilaments of all three proteins; a representative cross section of the ABB protofilament with the periodic repeat of ca. 40 nm is shown in Figure 5e.

Both ABBI and ABB-DF proteins developed extended networks of flexible fibrils (Figure 6b,c), exhibiting a significant variability in their morphology like fibrils assembled from other amyloidogenic proteins (*29*). Their *z* height varied from 2 to 12 nm, and the length sometimes exceeded a few micrometers. They were characterized by their tubular appearance and consisted of a few twisted substructures or protofilaments. The edge split of a single fibril into protofilaments with a characteristic height of 2 nm is shown in Figure 6b. The periodicity along the fibrillar axis spanned the range of 20−70 nm, which corresponded to the different tautness of protofilaments twisting around each other in response to the packing constraints imposed by twisted neighbors (*30*). It was suggested that the chiral twist of fibrils defines their finite width (*30*). In our samples, the periodicity of twist depended on the number of protofilaments in the fibril; the fibrils with *z* heights of ∼12 and ∼5 nm were characterized by repeat periodicities of ∼70 and ∼40 nm, respectively. In the cross-section analysis in Figure 6b, we have shown that the *z* height of the individual ABBI fibril can change along its axis from ∼4.5 to ∼3 nm and to ∼2 nm, consequently, indicating that the shorter protofilaments can wind around the longer carrier. Some short protofilaments remained in the samples of ABB constructs even after significantly longer periods of several weeks (Figure 6c).

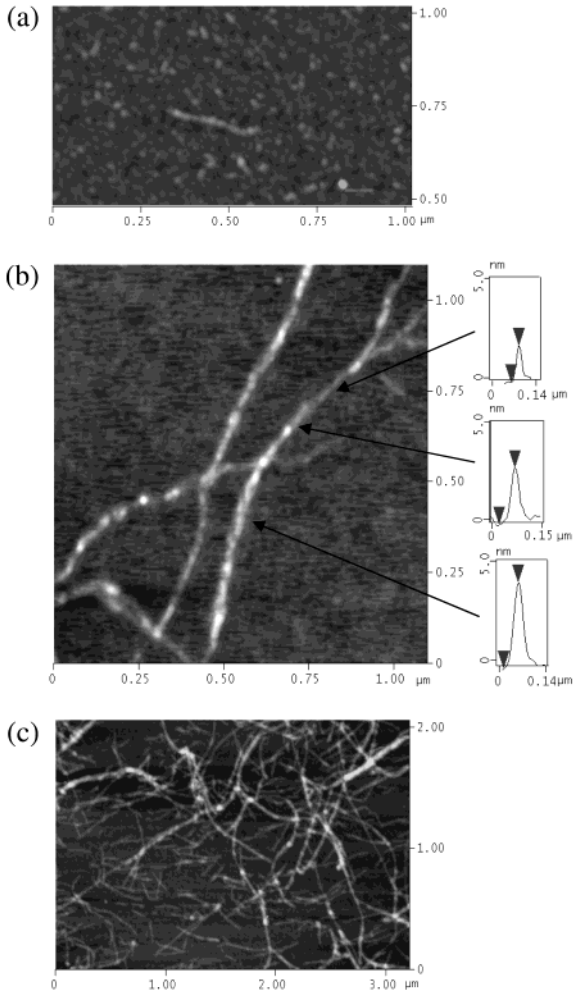

FIGURE 6: Amyloid structures of ABB constructs observed by AFM. (a) Height image of the ABBI sample after incubation for 2 h at pH 7.3 and 57 °C, with a *z* scale of 5 nm. Pivotal oligomers ca. 1.2 nm in height, chain, and ring assemblies are shown in lighter colors; the stretches of protofibrils and amyloid-prone oligomers ca. 2 nm in height are shown in brighter color. (b) Image of ABBI fibril demonstrating a variable height along its axis; the right panel shows the cross sections made perpendicular to the fibrillar axis relative to the mica substrate and marked by cursors. The *z* scale is 10 nm. (c) Height image of the network of ABB-DF fibrils after incubation for 3 days, with a *z* scale of 15 nm.

At room temperature in all samples, the round oligomers were formed rapidly, being present as dominant species up to day 4. During further incubation of ABB, the oligomers were not transformed into protofilaments as at 57 °C; instead, the enlarged granules with amorphous edges and a *z* height of ≥4 nm emerged and remained in the sample even after 24 days (Figure 5f). In the samples of ABBI and ABB-DF, the mature fibrils similar to those shown in panels b and c of Figure 6 were formed after incubation for 4 days and remained unchanged during the longer period of 24 days.

When ABB, ABBI, and ABB-DF were incubated at pH 7.3 and 57 °C in the presence of the HLDF-6 peptide, we did not observe any effect of the peptide on the morphology of ABBI and ABB-DF fibrils, while ABB formed significantly longer and thicker fibrils (Figure 5h), similar to those observed in the samples of the constructs (Figure 6b,c). HLDF-6 itself taken at a concentration of 20 mg/mL did not polymerize and remained soluble at both 23 and 57 °C during the incubation for 3−4 weeks.

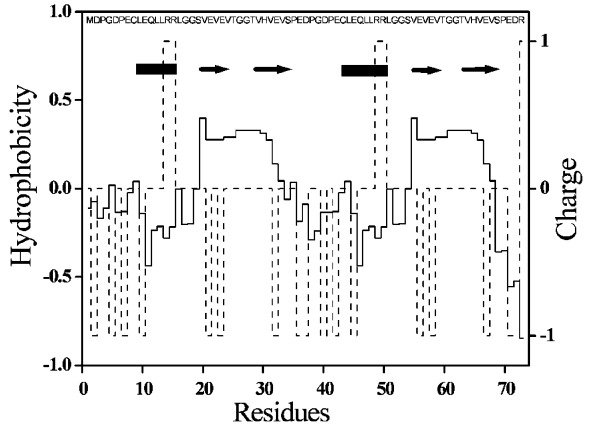

FIGURE 7: Hydrophobicity profile of the ABB amino acid sequence calculated using Eisenberg's consensus scale (*43*). Positive and negative values indicate hydrophobicity and hydrophilicity, respectively. α-Helices and β-strands are shown with bars and arrows, respectively. The dashed line shows the location of positive and negative charges (±1) in the amino acid sequence. The polypeptide sequence of ABB is presented at the top of the figure.

In the presence of 100 and 200 mM NaCl, the structural features of ABBI and ABB-DF fibrils did not change, while the morphology of ABB fibrils (Figure 5g) resembled those formed by ABB constructs (Figure 6b,c) or by ABB in the presence of HLDF-6 (Figure 5h).

DISCUSSION

Intrinsic Amyloidogenicity of ABB Proteins. Role of Electrostatic Interactions in Amyloid Formation. The results of this paper demonstrate that the carrier-protein ABB and its constructs readily self-assemble into a variety of amyloid structures at physiological pH. The design preventing ABB from aggregation was achieved by introducing 22 charged amino acid residues (17 Glu and Asp residues and 5 Arg and Lys residues) throughout the protein primary structure, creating a high net charge of −12 (http://www.expasy.org/tools/protparam.html). The large electrostatic repulsion contributes, though, to an overall instability of ABB, which is characterized by the conformational mobility of the molten globule type, and that can facilitate adoption of an alternative amyloid-prone fold.

The β-sheet region of ABB is characterized by the highest hydrophobicity within the amino acid sequence, as shown in the hydrophobicity plot (Figure 7). Thus, it can be a primary candidate for formation of the fibrillar cross-β-sheet. In the quadruple mutant of ribosomal S6 protein characterized by a similar fold, the β-sheet in the amyloid tetramer is also built up by the β-strands from the native protein (*31*). The cross-β-sheet is usually a very stable structure (*32*, *33*), suggesting that the intrinsically unstable building blocks of ABB should undergo structural conversion to integrate into fibrils. Indeed, the intact β-sheet of ABB would satisfy the principles of the "negative design" providing unsticky edges for the fibrillar assembly (Figures 1 and 2a). The two inner β-strands of the β-sheet of ABB carry a charge of −1 each, while the outer β-strands are characterized by a charge of −2 each. An inward-pointed charged side chain on the edge of the *de novo* β-sheet (*34*) as well as the gate-keeping consecutive charges of Asp61/62 and Arg46/47 in the S6 structure (*31*) was suggested to prevent amyloid formation. In the hexapeptide amyloid assembly, it has been shown though that the optimal peptide charges would be ±1 (*35*), while the solely hydrophobic interactions would lead to a rapid unstructured aggregation. To produce fibrils from ABB, we heated the sample to 57 °C. The heating neither leads to changes in the ABB secondary structure, as has been shown by far-UV CD (Figure 3b), nor increases the surface hydrophobicity as shown by ANS binding. The structural fluctuations of a very flexible ABB molecule occurring at higher temperatures can, however, increase the accessibility of the stickier inner β-strands promoting amyloid assembly.

It is remarkable that the fusion to the N-terminus of ABB of the short polar peptides significantly enhances the amyloidogenicity of ABB, increasing the kinetics of oligomerization (the lag phase disappeared), the rate of fibrillation (increasing the slope of ThT fluorescence time dependence during the assembly stage), promoting elongation of protofilaments and their lateral assembly into mature fibrils. These altogether are manifested in the formation of the dense fibrillar network (Figures 4 and 6). In ABBI, the insertion of the LKEKKYSP octapeptide stabilizes the ABB molecule (*13*), which can be considered an unfavorable factor for amyloid formation. Under the conditions of our experiments, the net charge of the interferon octapeptide is +2 and the net charge of HLDF-6 peptide is zero, though it bears one Arg. Being nonamyloidogenic itself, HLDF-6 equally promotes fibrillation of the carrier-molecule ABB whether it is covalently linked or present free in solution. The ABB model demonstrates that the β-sheet interface is easily accessible to the peptides (Figure 2a), which can counterbalance electrostatic repulsion of six Glu residues located in this amyloid assembly critical region. This is why an increased ionic strength produces a qualitatively similar effect on the kinetics (Figure 4b) and morphology of amyloid assembly (Figure 5g); however, the effect of the peptides is more pronounced. In addition, the peptides contain aliphatic groups which can provide a hydrophobic contribution to the peptide−protein interactions, stabilizing the fibrillar interface.

It is noteworthy that there are a few proteins with the topology based on an antiparallel β-sheet covered by two α-helices which form amyloid fibrils, including acylphosphatase (*36*), the S6 quadruple mutant (*31*), and the wild-type S6 protein (our unpublished results, the fibrillation at pH 2.0 and elevated temperatures), indicating that the amyloid-prone conformation can be evoked in this fold. Among them, ABB is the most charged protein. These results demonstrate that the gatekeeping electrostatic interactions within the hydrophobic sequences (*31*) can be effectively mediated by adding or fusing countercharged molecules or by changing environmental conditions such as ionic strength or temperature.

Model of ABB Fibrillogenesis. Oligomeric Intermediates and Fibrillation Pathways. The fibrillation of the ABB proteins, as shown in Figure 8, is a multiple-step process, including more than one intermediate preceding fibril formation. The initial oligomerization involves an association of the ABB monomers into the pivotal oligomers ca. 1.2 nm in height, containing 10−12 monomers. These species do not bind ThT, indicating the lack of the cross-β-sheet of a typical amyloid, and correspond to a lag phase in the time dependence of amyloid formation. They serve as a pivotal point leading to a few separate pathways.

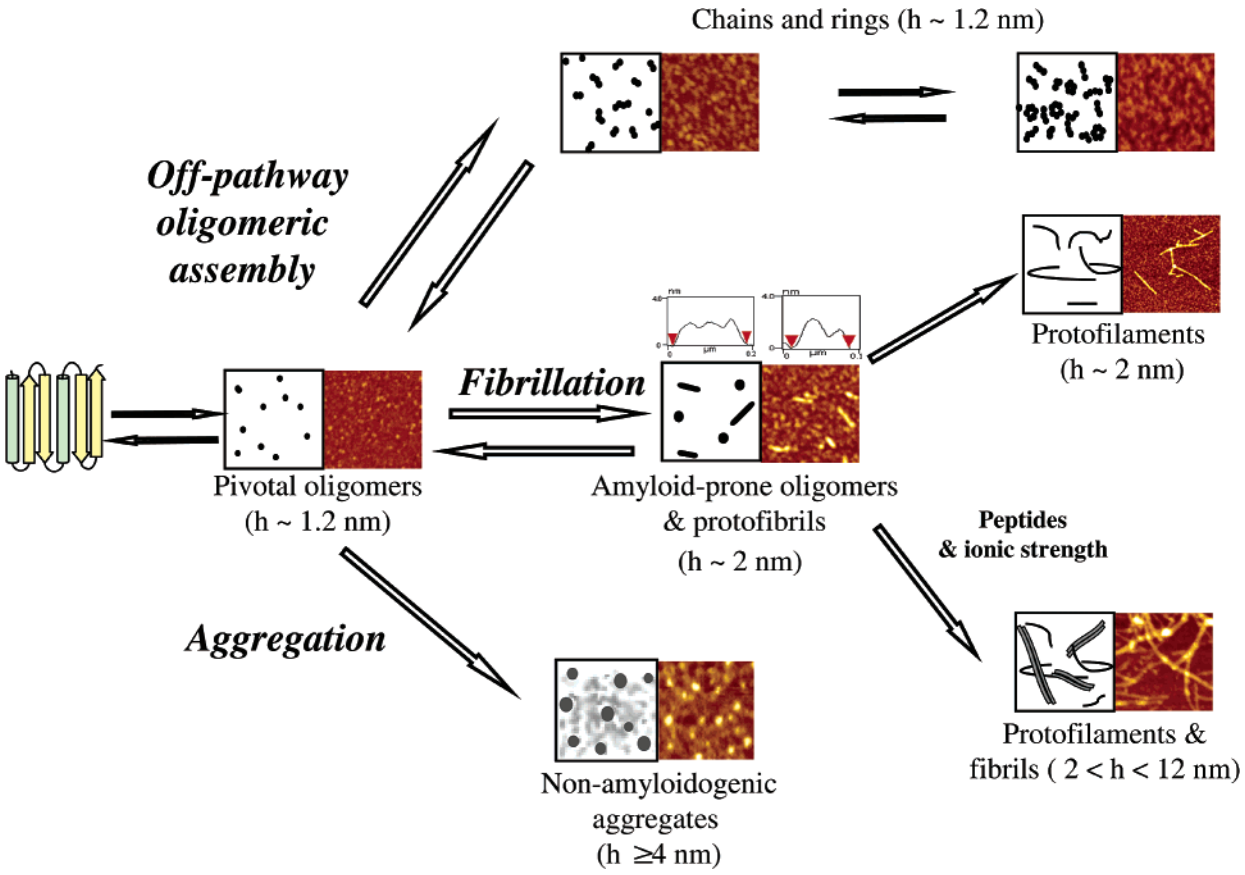

FIGURE 8: Model of ABB fibrillogenesis. Each graph shows the schematic presentation of the species (left) and the corresponding AFM image (right). Arrows indicate favorable pathways.

At room temperature, they assemble into the larger granular aggregates (a height of ≥4 nm), which do not form amyloid. At 57 °C, the top path in Figure 8, these oligomers become linked together into the linear chains with a well-defined bead-on-string morphology (*37*). The dimensions of constituting beads remain very similar whether they are present as individual oligomers or as a part of the chains. The circularization apparently stabilizes the chain structures, protecting their edges from assembly and disassembly and preventing them from being converted into protofilaments.

The beginning of the assembly phase in the kinetics of ABB amyloid formation (Figure 4) coincides with an appearance of the round oligomers of a larger size (ca. 2 nm in height) comprised of 26−30 molecules. At this stage the short protofibrils also emerged, indicating that a critical size of oligomers requires initiation of an extended β-sheet pattern. In cross-sectional analysis of the protofibrils, the well-distinguished segments can be identified by measuring oscillation of the heights along the axis, giving maxima of ca. 2 nm, which is consistent with assembly via oligomeric intermediates (*38*, *39*). In some protofibrils, we observed neighboring segments with ca. 2 and 1.2 nm maxima (Figure 8). This suggests that the elongation of protofibrils can occur through association of both types of oligomers. Given that the larger species are involved, they can initiate the transformation of the latter into the cross-β-sheet type structures.

At the stationary phase of the fibrillation of all three proteins, the round oligomers 1.2 nm in mean height, the chains and the rings are not consumed. Apparently, the proportion of the rings versus the chains increases with incubation time (Figure 5b,c). This indicates that they are off-pathway assemblies. To transform these structures into β-sheet-containing protofilaments, a significant free energy barrier should be overcome. This could be a reason that ABB does not polymerize at room temperature while the pivotal oligomers ca. 1.2 nm in height are formed. An increase in temperature effectively lowers the energy barrier, facilitating transformation of the smaller oligomers into the amyloid-prone ones, which indicates that this can be a limiting stage in amyloid assembly.

CONCLUSIONS

The ABB-type molecules were designed for biomedical applications; however, they have proven to be a valuable model for amyloid formation. ABB and the constructs form a hierarchy of amyloid structures, including two distinct types of oligomeric intermediates. Under appropriate conditions, the pivotal oligomers can give rise to chain and ring-type oligomeric assemblies. The on-pathway amyloid-prone oligomers are coupled with formation of cross-β-sheet structure and fibrillar growth. The inherent amyloidogenicity of ABB can be easily modulated by grafted polypeptide sequences and by environmental conditions, resulting in the population of a dominant amyloidogenic species of a certain type. That can lead to important implications because the on-pathway oligomers of proteins, either involved in neurodegenerative diseases (*40*) or not related to human pathologies, are considered to be cytotoxic (*41*). In the field of newly designed polypeptide-based therapeutics, the amyloidogenicity of protein products can create a new "hazardous" functionality not foreseen by the initial design and should be identified prior to their application.

ACKNOWLEDGMENT

We thank Michael Oliveberg for providing the S6 protein, Andrey Shchukarev for latex samples, and Alexander Talyzin for carbon nanotubes.

REFERENCES

1. Ryu, D. D., and Nam, D. H. (2000) Recent progress in biomolecular engineering, *Biotechnol. Prog. 16*, 2−16.
2. Torchilin, V. P., and Lukyanov, A. N. (2003) Peptide and protein drug delivery to and into tumors: challenges and solutions, *Drug Discovery Today 8*, 259−266.
3. Dobson, C. M. (2003) Protein folding and misfolding, *Nature 426*, 884−890.
4. Morozova-Roche, L. A., Zurdo, J., Spencer, A., Noppe, W., Receveur, V., Archer, D. B., Joniau, M., and Dobson, C. M. (2000) Amyloid fibril formation and seeding by wild-type human lysozyme and its disease-related mutational variants, *J. Struct. Biol. 130*, 339−351.
5. Malisauskas, M., Zamotin, V., Jass, J., Noppe, W., Dobson, C. M., and Morozova-Roche, L. A. (2003) Amyloid protofilaments from the calcium-binding protein equine lysozyme: formation of ring and linear structures depends on pH and metal ion concentration, *J. Mol. Biol. 330*, 879−890.
6. Hamada, D., and Dobson, C. M. (2002) A kinetic study of β-lactoglobulin amyloid fibril formation promoted by urea, *Protein Sci. 11*, 2417−2426.
7. Fandrich, M., Fletcher, M. A., and Dobson, C. M. (2001) Amyloid fibrils from muscle myoglobin, *Nature 410*, 165−166.
8. Dolgikh, D. A., Fedorov, A. N., Chermeris, V. V., Chernov, B. K., Finkel'shtein, A. V., Shul'ga, A. A., Alakhov, I. B., Kirpichnikov, M. P., and Ptitsyn, O. B. (1991) Preparation and study of albebetin, an artificial protein with a given spatial structure, *Dokl. Akad. Nauk SSSR 320*, 1266−1269.
9. Fedorov, A. N., Dolgikh, D. A., Chemeris, V. V., Chernov, B. K., Finkelstein, A. V., Schulga, A. A., Alakhov, Y. B., Kirpichnikov, M. P., and Ptitsyn, O. B. (1992) *De novo* design, synthesis and study of albebetin, a polypeptide with a predetermined three-dimensional structure. Probing the structure at the nanogram level, *J. Mol. Biol. 225*, 927−931.
10. Bocharova, O. V., Moshkovskii, S. A., Chertikova, R. V., Abdullaev, Z. Kh., Kolesanova, E. F., Dolgikh, D. A., and Kirpichnikov, M. P. (2002) Introduction of biologically active fragments of interferon-α_2 and insulin into the artificial protein albebetin affects immunogenicity of the final construct, *Mol. Biol. 6*, 84−90.
11. Nagarsekar, A., and Ghandehari, H. (1999) Genetically engineered polymers for drug delivery, *J. Drug Targeting 7*, 11−32.
12. Schwartz, J. J., and Zhang, S. (2000) Peptide-mediated cellular delivery, *Curr. Opin. Mol. Ther. 2*, 162−167.
13. Aphasizheva, I. Y., Dolgikh, D. A., Abdullaev, Z. K., Uversky, V. N., Kirpichnikov, M. P., and Ptitsyn, O. B. (1998) Can grafting of an octapeptide improve the structure of a *de novo* protein? *FEBS Lett. 425*, 101−104.
14. Chertkova, R. V., Kostanian, I. A., Astapova, M. V., Surina, E. A., Dolgikh, D. A., and Kirpichnikov, M. P. (2003) An artificial protein, possessing biological activity of HL-60 human promyelocytic leukemia differentiation factor, *Bioorg. Khim. 29*, 30−37.
15. Dolgikh, D. A., Uversky, V. N., Gabrielian, A. E., Chemeris, V. V., Fedorov, A. N., Navolotskaya, E. V., Zav'yalov, V. P., and Kirpichnikov, M. P. (1996) The *de novo* protein with grafted biological function: transferring of interferon blast-transforming activity to albebetin, *Protein Eng. 9*, 195−201.
16. Kostanyan, I. A., Astapova, M. V., Starovoytova, E. V., Dranitsina, S. M., and Lipkin, V. M. (1994) A new human leukemia cell 8.2 kDa differentiation factor: isolation and primary structure, *FEBS Lett. 356*, 327−329.
17. Guex, N., and Peitsch, M. C. (1997) SWISS-MODEL and the Swiss-PdbViewer: an environment for comparative protein modeling, *Electrophoresis 18*, 2714−2723.
18. Ginalski, K., Elofsson, A., Fischer, D., and Rychlewski, L. (2003) 3D-Jury: a simple approach to improve protein structure predictions, *Bioinformatics 19*, 1015−1018.
19. Edman, M., Berg, S., Storm, P., Wikstrom, M., Vikstrom, S., Ohman, A., and Wieslander, A. (2003) Structural features of glycosyltransferases synthesizing major bilayer and nonbilayer-prone membrane lipids in *Acholeplasma laidlawii* and *Streptococcus pneumoniae*, *J. Biol. Chem. 278*, 8420−8428.
20. Levine, H. (1993) Thioflavine-T interaction with synthetic Alzheimers-disease β-amyloid peptides: detection of amyloid aggregation in solution, *Protein Sci. 2*, 404−410.
21. Levine, H. (1995) Thioflavine-T interaction with amyloid β-sheet structures, *Amyloid 2*, 1−6.
22. Klunk, W. E., Pettegrew, J. W., and Abraham, D. J. (1989) Quantitative evaluation of Congo red binding to amyloid-like proteins with a β-pleated sheet conformation, *J. Histochem. Cytochem. 37*, 1273−1281.
23. Klunk, W. E., Pettegrew, J. W., and Abraham, D. J. (1989) Two simple methods for quantifying low-affinity dye-substrate binding, *J. Histochem. Cytochem. 37*, 1293−1297.
24. Chan, B. M. C., and Brash, J. L. (1981) Conformational changes in proteins adsorbed on polymer surface, *J. Colloid Interface Sci. 84*, 263−265.
25. Zhang, H., Bremmell, K., Kumar, S., and Smart, R. S. (2004) Vitronectin adsorption on surfaces visualized by tapping mode atomic force microscopy, *J. Biomed. Mater. Res. 68A*, 479−488.
26. Schneider, S. W., Larmer, J., Henderson, R. M., and Oberleithner, H. (1998) Molecular weights of individual proteins correlate with molecular volumes measured by atomic force microscopy, *Pfluegers Arch. 435*, 362−367.
27. Geisse, N. A., Wasle, B., Saslowsky, D. E., Henderson, R. M., and Edwardson, J. M. (2002) Syncollin homo-oligomers associate with lipid bilayers in the form of doughnut-shaped structures, *J. Membr. Biol. 189*, 83−92.
28. Morozova-Roche, L. A., Arico-Muendel, C. C., Haynie, D. T., Emelyanenko, V. I., Van Dael, H., and Dobson, C. M. (1997) Structural characterisation and comparison of the native and A-states of equine lysozyme, *J. Mol. Biol. 268*, 903−921.
29. Chamberlain, A. K., MacPhee, C. E., Zurdo, J., Morozova-Roche, L. A., Hill, H. A., Dobson, C. M., and Davis, J. J. (2000) Ultrastructural organization of amyloid fibrils by atomic force microscopy, *Biophys. J. 79*, 3282−3293.
30. Aggeli, A., Nyrkova, I. A., Bell, M., Harding, R., Carrick, L., McLeish, T. C., Semenov, A. N., and Boden, N. (2001) Hierarchical self-assembly of chiral rod-like molecules as a model for peptide β-sheet tapes, ribbons, fibrils, and fibers, *Proc. Natl. Acad. Sci. U.S.A. 98*, 11857−11862.
31. Otzen, D. E., Kristensen, O., and Oliveberg, M. (2000) Designed protein tetramer zipped together with a hydrophobic Alzheimer homology: a structural clue to amyloid assembly, *Proc. Natl. Acad. Sci. U.S.A. 97*, 9907−9912.
32. Serpell, L. C. (2000) Alzheimer's amyloid fibrils: structure and assembly, *Biochim. Biophys. Acta 1502*, 16−30.
33. Hirota-Nakaoka, N., Hasegawa, K., Naiki, H., and Goto, Y. (2003) Dissolution of β_2-microglobulin amyloid fibrils by dimethylsulfoxide, *J. Biochem. 134*, 159−164.
34. Richardson, J. S., and Richardson, D. C. (2002) Natural β-sheet proteins use negative design to avoid edge-to-edge aggregation, *Proc. Natl. Acad. Sci. U.S.A. 99*, 2754−2759.
35. Lopez De La Paz, M., Goldie, K., Zurdo, J., Lacroix, E., Dobson, C. M., Hoenger, A., and Serrano, L. (2002) *De novo* designed peptide-based amyloid fibrils, *Proc. Natl. Acad. Sci. U.S.A. 99*, 16052−16057.
36. Chiti, F., Webster, P., Taddei, N., Clark, A., Stefani, M., Ramponi, G., and Dobson, C. M. (1999) Designing conditions for *in vitro* formation of amyloid protofilaments and fibrils, *Proc. Natl. Acad. Sci. U.S.A. 96*, 3590−3594.
37. Lashuel, H. A., Hartley, D. M., Petre, B. M., Wall, J. S., Simon, M. N., Walz, T., and Lansbury, P. T., Jr. (2003) Mixtures of wild-type and a pathogenic (E22G) form of Aβ_{40} *in vitro* accumulate protofibrils, including amyloid pores, *J. Mol. Biol. 332*, 795−808.
38. Serio, T. R., Cashikar, A. G., Kowal, A. S., Sawicki, G. J., Moslehi, J. J., Serpell, L., Arnsdorf, M. F., and Lindquist, S. L. (2000) Nucleated conformational conversion and the replication of conformational information by a prion determinant, *Science 289*, 1317−1321.
39. Modler, A. J., Gast, K., Lutsch, G., and Damaschun, G. (2003) Assembly of amyloid protofibrils *via* critical oligomers: a novel pathway of amyloid formation, *J. Mol. Biol. 325*, 135−148.
40. Chromy, B. A., Nowak, R. J., Lambert, M. P., Viola, K. L., Chang, L., Velasco, P. T., Jones, B. W., Fernandez, S. J., Lacor, P. N., Horowitz, P., Finch, C. E., Krafft, G. A., and Klein, W. L. (2003) Self-assembly of A$\beta_{(1-42)}$ into globular neurotoxins, *Biochemistry 42*, 12749−12760.
41. Bucciantini, M., Giannoni, E., Chiti, F., Baroni, F., Formigli, L., Zurdo, J., Taddei, N., Ramponi, G., Dobson, C. M., and Stefani,

M. (2002) Inherent toxicity of aggregates implies a common mechanism for protein misfolding diseases, *Nature 416*, 507−511.
42. Koradi, R., Billeter, M., and Wüthrich, K. (1996) MOLMOL: a program for display and analysis of macromolecular structures, *J. Mol. Graphics 14*, 51−55.
43. Eisenberg, D., Schwarz, E., Komaromy, M., and Wall, R. (1984) Analysis of membrane and surface protein sequences with the hydrophobic moment plot, *J. Mol. Biol. 179*, 125−142.

BI0494121